J Mater Sci (2009) 44:4599–4603
DOI 10.1007/s10853-009-3701-7

Thermal stability and magnetic anisotropy of nickel nanoplates

Yonghua Leng · Jie Zheng · Jianglan Qu · Xingguo Li

Received: 26 March 2009 / Accepted: 19 June 2009 / Published online: 11 July 2009

Abstract The thermal stability and magnetic anisotropies of nickel nanoplates with {111} planes as the exposure plane are studied. The melting point of Ni nanoplates drastically drops as compared to that of the bulk one due to the significant increase in the surface free energy. For the large aspect ratio, these nanoplates tend to lie flat on silicon wafer and form a thin Ni {111} plane film. Both the coercivity and the remnant magnetization of the Ni film deeply depend on the applied field direction. As the angle between the film plane and the applied field direction varies from zero to 45° and to 90°, the coercivity measured at 5 K increases from 335 Oe to 373 and to 410 Oe. Correspondingly, the remnant magnetization decreases from 18.1 to 15.8 to be 10.4 emu/g.

Introduction

As important materials of choice, magnetic materials have attracted much attention for their wide applicability [1–5]. Nickel nanoparticles have been used as catalyst for carbon nanotubes growth [6–8], hydrogen generation [9], or hydrogenation reaction [10]. In addition, nano-scaled nickel material is also a promising potential as regards its application in perpendicular magnetic storage and medical diagnostics [11]. Compared with Fe and Co materials, bulk nickel has lower magnetization (55 emu/g [12]). Nielsch et al. [13] prepared high density nickel nanowire arrays, which show a coercive field of 1200 Oe and a squareness of nearly 100% when the magnetic field is applied parallel to the wire axis. Although the coercive force for bulk nickel was only 0.7 Oe, high coercive force of 2.7 kOe was obtained for the core–shell Ni/Au nanoparticles [14].

Metal nanoparticles often exhibit shape-dependent properties [15, 16]. For example, the catalytic performance has been shown to depend on the exact crystal plane. It has been demonstrated that the oxygen reduction reaction on Pt (100) is higher than that on Pt (111) owing to the different binding strength on these facets [17]. The nanoparticles with 2D structures are believed easy to control some chemical and physical properties due to their high aspect ratio. Many metal nanoplates with triangular and/or hexagonal morphologies, such as Au [18], Ag [19], Ni [20, 21], and Cu [22] have been successfully synthesized by various methods. Among these, both the surface-enhanced Raman scattering and surface plasma resonances have been studied well for the noble metals. It has also been revealed that for metallic materials the melting points show strong dependence on the particles size and the morphologies. For the non-spherical particles, their high surface free energy makes them melt at lower temperature [23]. Nickel materials are important catalysts. Therefore, it is important to determine the thermal stability of nickel nanoplates for their applications, especially when high temperature is desired. Moreover, the magnetic shape anisotropy caused by the plate structure has not been reported. In this article, we studied the thermal stability of nickel nanoplates and demonstrated their magnetic properties combined with their magnetocrystalline anisotropy and shape anisotropy.

Y. Leng · J. Zheng · J. Qu · X. Li
Beijing National Laboratory for Molecular Sciences (BNLMS), The State Key Laboratory of Rare Earth Materials Chemistry and Applications, College of Chemistry and Molecular Engineering, Peking University, Beijing 100871, China

X. Li (✉)
College of Engineering, Peking University, Beijing 100871, China
e-mail: xgli@pku.edu.cn

Experimental

Nickel nanoplates were prepared by thermal decomposition of nickel formate with the aid of $Fe(CO)_5$, as described in our previous articles [24, 25]. In order to measure the thermal stability of the 2D structures, the resulting nickel nanoplates were redispersed in 2 mL of cyclohexane to get a black suspension assisted by ultrasonication. Take one drop of the suspension onto a carbon-coated copper grid. After the first drop dried, another drop of the same suspension was added. This procedure was repeated for at least three times. In the same way, two copper grids coated with nickel nanoplates were prepared. One of the obtained copper grids was protected by aluminum foil and then slowly heated to 473 K in hydrogen and maintained at that temperature for 1 h. The other copper grid packed by aluminum foil was heated to 673 K and maintained for 0.5 h under hydrogen. Then, the morphology was investigated by transmission electron microscopy (TEM, JEOL JEM-200CX).

In order to prepare the sample for superconductive quantum interference device (SQUID) measurement, a silicon wafer of size 5 × 5 mm was cleaned with acetone by ultrasonication for 10 min. Subsequently, the cyclohexane suspension of the nanoplates was added dropwise to the silicon. Again, the suspension was not dropped until the former drop had been dried. This procedure was repeated until a thin layer was formed on the silicon wafer, which could be clearly observed by naked eyes. The magnetic properties were investigated by a SQUID. The magnetic data were recorded by varying the angular degrees between the applied external field and the surface of the silicon to be 0, 45, and 90°. A powder sample of the same Ni nanoplates in a gelatin capsule was measured by the same procedures for comparison.

Results and discussion

Thermal stabilities

The as-synthesized nickel nanoplates shown in Fig. 1a have the triangular or hexagonal shapes, which prefer to overlap together and lie flat on the substrate due to the strong magnetic interactions among different plates and their ultrathin nature. Selected area electron diffraction (SAED) pattern of a single nanoplate (either triangular or hexagonal) reveals that the nanoplates are single crystal with a (111) crystal plane as the bonded plane (not shown here).

After annealing at 473 K for 1 h under hydrogen, most of the nickel nanoplates having small edge lengths remained its original shapes and smooth surface, as shown in Fig. 1b and c. However, the surface became very coarse

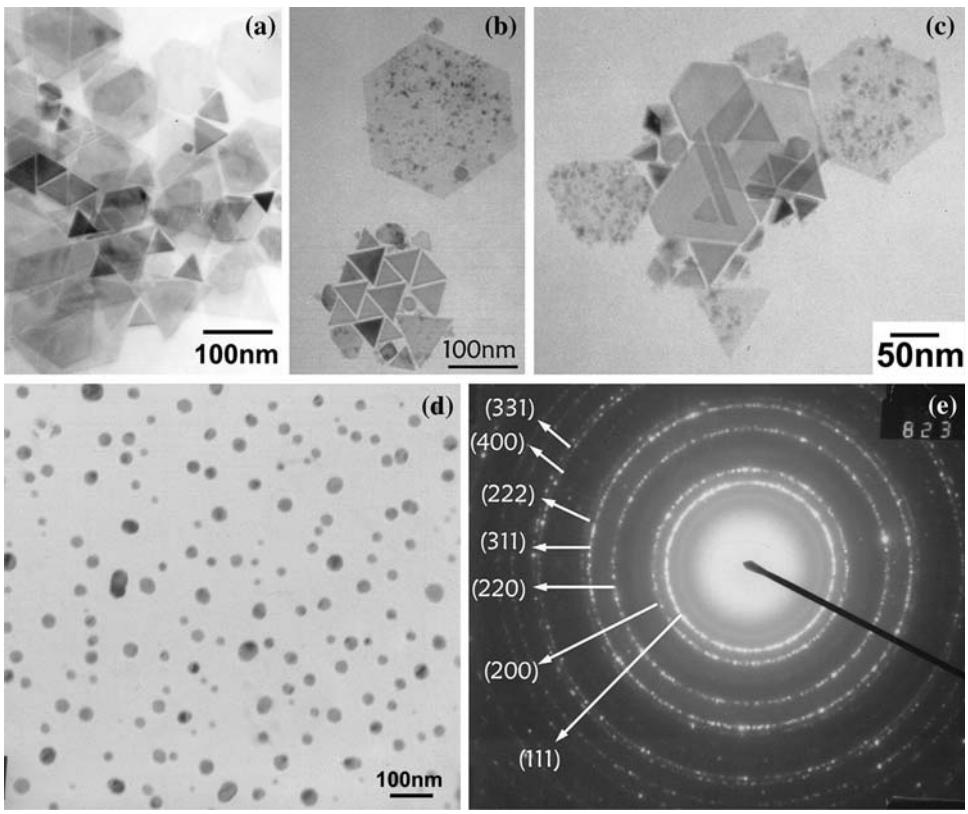

Fig. 1 TEM images of the nickel nanoplates **a** as-synthesized, **b–c** after annealing at 473 K for 1 h; **d** after annealing at 673 K for 0.5 h, and **e** the selected-area electron diffraction of particles in (**d**)

for the larger nickel nanoplates though keeping their plate-like structures. When the nickel nanoplates were annealed at 673 K for 0.5 h, no plate morphology could be observed. Instead, only nearly spherical nanoparticles with uniform size were present on the copper grid. SAED pattern shown in Fig. 1e confirmed that these small particles agreed well with the nickel metal phase, implying that these particles were the annealing products of nickel nanoplates. It is almost impossible for such small uniform nanoparticles to be obtained only by disintegrating the nanoplates into pieces. The only possibility is that the nanoplates undergo a melting process and then maintain the shape of liquid droplets during the cooling process. In fact, such an idea to obtain uniform particles by maintaining the shapes of liquid droplets during quick cooling has been adapted for synthesis of monodispersed Pb spherical colloids [26]. This result reveals that the melting point of nickel is significantly decreased from 1726 K to less than 673 K after forming the plate morphology with high surface free energy.

Magnetic properties

The temperature-dependent magnetization curves (*M–T* curves) shown in Fig. 2 were measured using the zero-field-cooling (ZFC) and field-cooling (FC) modes from 5 to 300 K under an applied field of 500 Oe. All the curves indicate superparamagnetism behaviors. As the field direction is parallel to the silicon wafer surface (designated as S2), the film indicates a slight lower blocking temperature (T_B, 200 K), and a slightly higher magnetization than that of the same powder sample (designated as S1). With increased angle between the field direction and the silicon surface, T_B increases to be 236 K for 45° (designated as S3), and 258 K for 90° (designated as S4). Meanwhile, the magnetization decreases quickly with change of the field direction. The extent of magnetizing depends on the field direction, which also confirms the formation of nickel film with magnetic anisotropies on the silicon wafer.

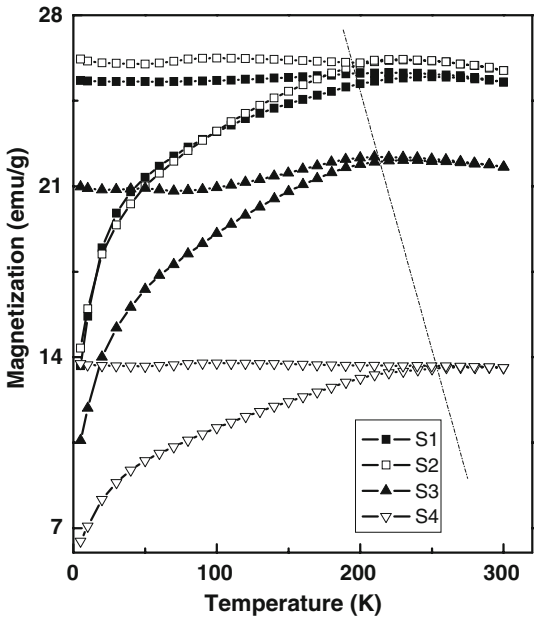

Fig. 2 ZFC and FC curves of the nickel film by varying the directions of the applied field compared to the powder sample

Figure 3 shows the *M* (*H*) curves measured at 5 K. With increasing angle between the wafer surface and the applied field direction, the hysteresis loops become much narrower. However, the saturation magnetizations (*Ms*) determined in all the cases are 40 emu/g, which account for 73% of the corresponding bulk value. The reduction in *Ms* compared to the bulk value may result from the thin nano-scaled thickness of the nanoplates.

As seen from Fig. 3, we may notice that all the loops are slightly shifted to the left side as a consequence of exchange bias (EB) between the ferromagnetic Ni and antiferromagnetic NiO [27]. Although NiO phase was not detected by SAED, a thin layer of NiO may coat on the surface of Ni nanoplates for the active feature of nanomaterials. The EB for S1 has been determined to be $H_{EB} = -11$ Oe. For the film sample, the largest H_{EB} for S2was found to be -18 Oe. This value decreased to be -17 Oe for S3 and -10 Oe for S4. The difference in H_{EB} should be related to the antiferromagnetic domain wall widths, which were dependent on the magnetic anisotropies [28]. The detailed data listed in Table 1 shows that the coercivity at 5 K was gradually increased from S1 to S4, confirming the strong magnetic anisotropy in the nickel-coated silicon wafer. Markedly, when the applied field was perpendicular to the surface of silicon, S4 has the highest value of 410 Oe, which is much higher than the powder composed of the randomly distributed nickel nanoplates. Although this value is smaller than the result, ~600 Oe for Ni nanowires with the diameters ranging from 40 to 100 nm and lengths up to 5 μm due to the latter's one-dimensional shapes [29], the coercivity for our nickel nanoplates was much higher than that of bulk nickel even though the thickness of our nanoplates was only 10 nm. It indicates that improved magnetic properties could not only be realized by the 1D structure, but can also be achieved from the 2D morphology. On the contrary, the remnant magnetizations gradually decreased from 18.1 for S2 to 15.8 for S3 and to 10.4 emu/g for S4, leading to the corresponding remnant ratio (M_r/M_s) changing from 47.0 to 39.3% and to 26.3%, respectively.

Considering that our nickel nanoplates have the (111) plane as the bounded planes and [111] direction is the easy axis for fcc Ni metal, it is easy to deduce that from S2 to S4, their magnetocrystalline anisotropy increases, and, in the meanwhile, the shape anisotropy decreases. The competition

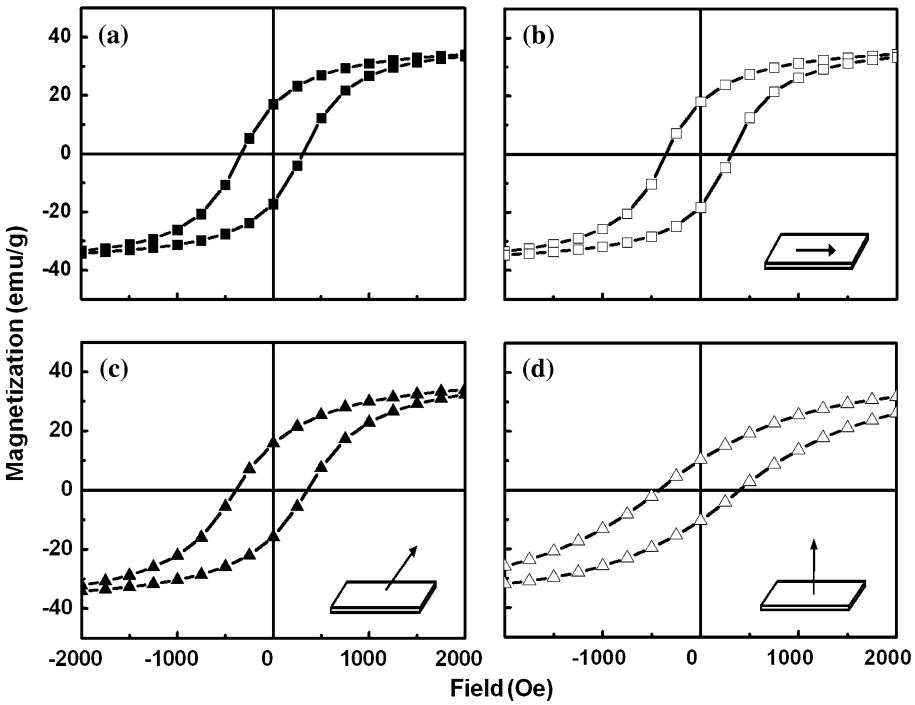

Fig. 3 Hysteresis loops for powder sample (**a**) and thin film with varied angles with the applied field direction **b** 0, **c** 45°, and **d** 90°

Table 1 Remnant magnetization and coercive forces obtained from Fig. 3

	S1	S2	S3	S4
H_c/Oe	322	335	373	410
H_{EB}/Oe	−11	−18	−17	−10
M_r/emu g^{-1}	17.0	18.1	15.8	10.4
M_r/M_s	44.3	47.0	39.3	26.3

between shape anisotropy and magnetocrystalline anisotropy should be responsible for the different chang tendencies for the coercivity and the remnant ratio with the variation direction of the applied field. It should be pointed out that this nickel film is quite different from the epitaxial FePt films where magnetocrystalline anisotropy is the dominant factor [30, 31]. In the case of S2, the shape anisotropy was dominant to determine the magnetic properties, leading to the highest remnant magnetism and the lowest coercivity. The magnetocrystalline anisotropy dominating for S4 should be responsible for the highest coercivity and the smallest remnant magnetism. Thus, for S3, both higher coercivity and remnant magnetism than the powder sample (S1) could be obtained for the remaining two kinds of magnetic anisotropies, leading to the maximum magnetic flux.

Conclusions

The thermal stability and magnetic properties for the thin nickel nanoplates have been studied. Their melting point deeply decreased due to the high surface energy of the plate structures. The coexistence and competition of magnetocrystalline and shape anisotropy caused the different change tendencies for the determined coercivity and the remnant magnetization.

Acknowledgements The authors acknowledge NSFC (Nos. 20671004 and 20821091), MOST of China (No. 2009CB939902), MOE of China (No. 707002) and Delta Electronics INC.

References

1. Liu DY, Ren S, Wu H, Zhang QT, Wen LS (2008) J Mater Sci 43:1974. doi:10.1007/s10853-008-2459-7
2. Talapatra S, Tang X, Padi M, Kim T, Vajtai R, Sastry GVS, Shima M, Deevi SC, Ajayan PM (2009) J Mater Sci 44:2271. doi:10.1007/s10853-008-3015-1
3. Kumagai H, Sobukawa H, Kurmoo M (2008) J Mater Sci 43:2123. doi:10.1007/s10853-007-2033-8
4. Liu Q, Huang H, Lai L, Sun J, Shang T, Zhou Q, Xu Z (2009) J Mater Sci 44:1187. doi:10.1007/s10853-009-3268-3
5. Wang HB, Northwood DO (2008) J Mater Sci 43:1050. doi:10.1007/s10853-007-2268-4
6. Gozzi D, Latini A, Capannelli G, Canepa F, Napoletano M, Cimberle MR, Tropeano M (2006) J Alloy Compd 419:32
7. Sanjabi S, Faramarzi A, Momen MH, Barber ZH (2009) J Phys Chem C 113:8652
8. Moshkalyov SA, Moreau ALD, Guttierrez HR, Cotta MA, Swart JW (2004) Mater Sci Eng B-Solid State Mater Adv Technol 112:147
9. Metin O, Ozkar S (2007) Int J Hydrogen Energy 32:1707
10. Mahata N, Cunha AF, Orfao JJM, Figueiredo JL (2009) Catal Commun 10:1203
11. Ding XZ, Wu XY, Chiah MC, Cheung WY, Wong SP, Wilson IH, Zhu XR, Shen HL, Liu XH (1999) J Appl Phys 85:8322

12. Sahoo Y, He Y, Swihart MT, Wang S, Luo H, Furlani EP, Prasad PN (2005) J Appl Phys 98:054308
13. Nielsch K, Wehrspohn RB, Barthel J, Kirschner J, Fischer SF, Kronmuller H, Schweinbock T, Weiss D, Gosele U (2002) J Magn Magn Mater 249:234
14. Chen D, Liu S, Li JJ, Zhao NQ, Shi CS, Du XW, Sheng J (2009) J Alloy Compd 475:494
15. Chen M, Kim J, Liu JP, Fan HY, Sun SH (2006) J Am Chem Soc 128:7132
16. Dumestre F, Chaudret B, Amiens C, Renaud P, Fejes P (2004) Science 303:821
17. Markovic NM, Gasteiger HA, Ross PN (1995) J Phys Chem 99:3411
18. Chu HC, Kuo CH, Huang MH (2006) Inorg Chem 45:808
19. Wu QS, Zhao Y, Zhang CB, Li F (2005) Acta Physica Sin 54:1452
20. Leng YH, Li Y, Li XG, Takahashi S (2007) J Phys Chem C 111:6630
21. Li DG, Ni XM, Zheng HG, Qi BH (2008) Chem Lett 37:148
22. Fan N, Xu LQ, Li J, Ma XC, Qian YT (2007) J Cryst Growth 299:212
23. Kan CX, Wang GH, Zhu XG, Li CC, Cao BQ (2006) Appl Phys Lett 88:071904
24. Leng YH, Zhang YH, Liu T, Suzuki M, Li XG (2006) Nanotechnology 17:1797
25. Leng YH, Wang YT, Li XG, Liu T, Takahashhi S (2006) Nanotechnology 17:4834
26. Wang YL, Cai L, Xia YN (2005) Adv Mater 17:473
27. Yi JB, Ding J, Zhao ZL, Liu BH (2005) J Appl Phys 97:10K306
28. Fraune M, Rudiger U, Guntherodt G, Cardoso S, Freitas P (2000) Appl Phys Lett 77:3815
29. Wernsdorfer W, Hasselbach K, Benoit A, Barbara B, Doudin B, Meier J, Ansermet JP, Mailly D (1997) Phys Rev B 55:11552
30. Matsumoto M, Morisako A, Katayama N (2003) J Appl Phys 93:7169
31. Sun SH, Murray CB, Weller D, Folks L, Moser A (2000) Science 287:1989